Mechanism of the enhancing effect of glycyrrhizin on nifedipine penetration through a lipid membrane

A.V. Kim [a,b,*], E.A. Shelepova [a], V.I. Evseenko [c], A.V. Dushkin [c], N.N. Medvedev [a,b], N.E. Polyakov [a,c]

[a] Institute of Chemical Kinetics and Combustion, Institutskaya St., 3, 630090 Novosibirsk, Russia
[b] Novosibirsk State University, Novosibirsk, Russia
[c] Institute of Solid State Chemistry and Mechanochemistry, Novosibirsk, Russia

ARTICLE INFO

ABSTRACT

The saponin glycyrrhizin from liquorice root shows the ability to enhance the therapeutic activity of other drugs when used as a drug delivery system. Due to its amphiphilic properties, glycyrrhizin can form self-associates (dimers, micelles) and supramolecular complexes with a wide range of hydrophobic drugs, which leads to an increase in their solubility, stability and bioavailability. That is why the mechanism of the biological activity of glycyrrhizin is of considerable interest and has been the subject of intensive physical and chemical research in the last decade. Two mechanisms have been proposed to explain the effect of glycyrrhizin on drug bioavailability, namely, the increase in drug solubility in water and enhancement of the membrane permeability. Interest in the membrane-modifying ability of glycyrrhizic acid (GA) is also growing at present due to its recently discovered antiviral activity against SARS-CoV-2 Bailly and Vergoten (2020) [1]. In the present study, the passive permeability of the DOPC lipid membrane for the calcium channel blocker nifedipine was elucidated by parallel artificial membrane permeability assay (PAMPA) and full atomistic molecular dynamics (MD) simulation with free energy calculations. PAMPA experiments show a remarkable increase in the amount of nifedipine (NF) permeated with glycyrrhizin compared to free NF. In previous studies, we have shown using MD techniques that glycyrrhizin molecules can integrate into the lipid bilayer. In this study, MD simulation demonstrates a significant decrease in the energy barrier of NF penetration through the lipid bilayer in the presence of glycyrrhizin both in the pure DOPC membrane and in the membrane with cholesterol. This effect can be explained by the formation of hydrogen bonds between NF and GA in the middle of the bilayer.

© 2021 Elsevier B.V. All rights reserved.

1. Introduction

Over the past decade, various physicochemical approaches have been increasingly employed to explore the detailed mechanisms of the biologically relevant processes. One of the most challenging tasks of modern pharmaceutical science involves attempts to increase the drug efficiency and at the same time reduce their toxicity. A promising way to create novel and more powerful forms is the preparation of molecular complexes of the existing drugs with an appropriate carrier or drug delivery system (DDS) [see, for example, [2,3,5,6]]. Such systems are capable of facilitating drug

delivery, protecting the parent substances from metabolic degradation, and promoting their prolonged action.

Glycyrrhizin or β-Glycyrrhizic acid (GA, Fig. 1), a triterpene glycoside extracted from liquorice root, is a novel and promising carrier that has been shown to reduce the toxicity and increase the therapeutic activity of a variety of essential antibiotics and cardiovascular preparations [see reviews [7–11]]. For example, the complexes of GA with antiarrhythmic drug nifedipine show a significant increase in its therapeutic activity in the models of adrenaline-induced hypertension and $CaCl_2$-induced arrhythmia [12]. Nifedipine (NF, 1,4-dihydro-2,6-dimethyl-4-(2′-nitrophenyl)-3,5-pyridinedicarboxylic acid dimethyl ester, Fig. 1) is one of the commonly used calcium channel blockers. Taking into account the published data on the decrease in heart pressure with the use of GA [13], a synergistic effect can be expected from the use of the GA/NF complex. From our point of view, in order to understand the reasons underlying the above-mentioned effect, it is necessary to
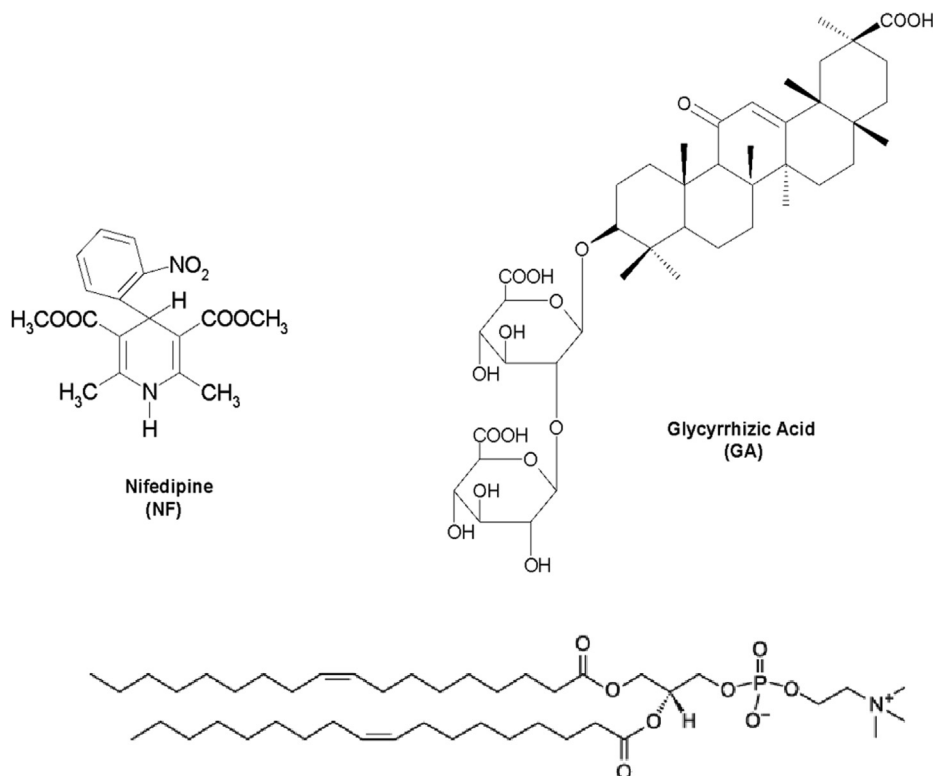
Fig. 1. Structural formulas of nifedipine (NF), glycyrrhizic acid (GA), and 1,2-dioleoyl-*sn*-glycero-3-phosphocholine (DOPC).

study the molecular-level mechanisms of the impact of DDS on drug activity.

In our earlier papers, we demonstrated the ability of GA to form water-soluble supramolecular associates with a variety of lipophilic drugs [14–22]. It has been shown that such complexes are characterized by increased solubility, stability, and bioavailability. NMR relaxation, MASS spectroscopy, and gel-permeation chromatography has shown that, due to their amphiphilic properties, GA molecules can form self-associates and micelles in water solutions – the precursors of 'host–guest' inclusion complexes [23–27]. Various physicochemical studies have demonstrated an increase in the chemical and photostability of "guest" molecules in such complexes [20–23].

The membrane modifying ability of GA has been described recently [28–33]. Thus, an additional mechanism of GA's influence on the drug bioavailability was suggested, namely, an increase in membrane permeability. Membrane permeability should be a key metric in the design of new drug formulations. Most drugs need to pass through at least one cell membrane, and low membrane permeability often results in poor *in vivo* efficacy.

Numerous methods are used to estimate the extent of drug absorption through the human gastrointestinal wall, from relatively simple physical techniques to highly expensive cell-based approaches [34]. Among these, the cell-free permeation systems, including the parallel artificial membrane permeation assay (PAMPA), are attracting significant attention due to a reliable prediction ability of passive intestinal absorption without the disadvantages of cell- or tissue-based methods. PAMPA enabled the fast determination of the ability of the compounds to permeate a membrane by passive diffusion and thus was suitable for screening potential drugs [35]. The PAMPA in vitro technique was developed in 1998 by Kansy et al. [36] and established initially to rapidly predict passive permeability through the gastrointestinal tract, but now has been adapted for use in other systems, including the

blood–brain barrier [37,38]. Briefly, the technique involves a donor and an acceptor compartment separated by a filter supporting a liquid artificial membrane. The model membrane can be composed of a variety of phospholipid mixtures. The tested compound is placed in the donor compartment and allowed to pass into the acceptor compartment through the artificial membrane.

The present paper describes the results of the membrane permeability study for the NF molecule using the model DOPC lipid membrane (Fig. 1). For this purpose, we applied a combination of the experimental method of parallel artificial membrane permeability assay (PAMPA) and molecular dynamics (MD) simulation.

The work described here demonstrates robust consistency between previous NMR data, new PAMPA experiments, and the predictive capacity of MD calculations. Also, the NF penetration through a more complex membrane containing cholesterol (CLR) was simulated, and the effect of GA on permeation was examined.

One of the most powerful *in silico* techniques to simulate the molecular process of diffusion at the atomic level is molecular dynamics [39]. Some works combine the MD simulations with the PAMPA experiment [37,40]. Coupling MD with free energy techniques provides a powerful tool to study membrane permeability in detail. Since phosphatidylcholine lipids are the major phospholipids within cellular membranes, a single bilayer can provide a good first approximation of the physicochemical properties of a cell membrane; cholesterol could also be added.

In the present study, the MD simulation technique was applied to find out whether GA molecules help NF to pass through lipid membranes and to elucidate the molecular mechanism of such a process. We performed the full-atomistic molecular dynamic simulation of the lipid bilayer DOPC containing one GA molecule to calculate the potential of mean force (PMF) for permeation of a nifedipine molecule through the bilayer in the presence and absence of GA.

2. Experimental section and methods

2.1. Chemicals and preparation of the complex

Nifedipine (NF, 1,4-dihydro-2,6-dimethyl-4-(2′-nitrophenyl)-3, 5-pyridinedicarboxylic acid dimethyl ester, Sigma) and Glycyrrhizic acid (GA), a saponin from Licorice root (98%, Shaanxi Pioneer Biotech Co., Ltd., China), were used as supplied. GA-NF mixture (2:1-mole ratio) for PAMPA experiments was prepared by the mechanical treatment of solid NF with GA in the planetary mill [14,17,18]. Type of mill: AGO-2. Processing mode: acceleration of grinding media 20 g (free fall), mass 2.0 g, drum capacity 50 mL, grinding media-steel balls (diameter 6 mm, 75.0 g load), processing time were 5 and 10 min, respectively.

2.2. Solubility study

To determine the solubility of GA/NF complex, the amount of 0.12 g of the obtained solid GA/NF complex, or 0.02 g of free nifedipine was dissolved in 10 mL of distilled water in a shaker-incubator (37 °C, 200 rpm) for 3 h. In all cases, the drug in solution was in equilibrium with the undissolved one. After that, the solution was centrifuged (12000 r/min, 10 min) and filtered through a paper filter. The drug concentration in the solution was determined by HPLC chromatograph Agilent 1200 with column Zorbax Eclipse XDB-C18, 4.6·50 mm at RT (27 °C), and diode-array detector. Acetonitrile - acetate buffer (55:45) was used as eluent, pH = 3.4, flow rate = 0.9 mL/min, sampling 5 μL, detection wavelength 240 nm. The concentration of NF was determined using its specially prepared calibration solutions in ethanol.

2.3. In vitro parallel artificial membrane permeability assay (PAMPA)

The PAMPA model is a method for predicting passive intestinal absorption [36,41]. PAMPA experiment is carried out in 12-well filter plates (polycarbonate membrane, 12 mm diameter inserts, 0.4 μm pore size, 1.12 cm^2 area, Corning Incorporated). The ability of compounds to diffuse from the donor compartment to the acceptor compartment is evaluated. The artificial membrane was first impregnated by carefully pipetting 60 μL of the 5% (v/v) (2% DOPC in hexadecane) in hexane solution into each well of the donor plate. The wells were then placed into a fume hood for 1 h to ensure complete evaporation of hexane. After evaporation of the hexane, 1.5 mL of water was added to each well of the acceptor plate. The DOPC treated donor plate was then placed on top of the 12-well acceptor plate. Then 0.5 mL of nifedipine or its complex with GA in water (concentration of GA is 0.5, 1, and 5 mM) was added to each well of the donor plate, and the resulting PAMPA device was incubated at 37 °C and shaken for 2.5 h at 200 rpm. Samples (1 mL) were collected from the acceptor plate at the appropriate time points (15, 30, 45, 60, 75, 90, 105, 120, 135, 150 min) and analyzed by HPLC, and the same volume of fresh medium was replenished.

2.4. Molecular dynamics (MD) simulation

All simulations were carried out using the GROMACS package v. 2016. We used the same parameter sets and protocol as in our previous papers [28,32]. Berger's DOPC lipids [42] were employed in GROMOS53a6 forcefield. Glycyrrhizic acid (GA), nifedipine (NF), and cholesterol (CLR) molecules topologies were generated by Automated Topology Builder service [43] based on GROMOS53a6 force field. The water model is SPC [44]. The composition depends on the model and consists of 0–1 NF molecules, 0–2 GA molecules, 128 or 114 DOPC lipid molecules, 0 or 14 CLR molecules and about 5000–7000 water molecules. The detailed information about all the model compositions is in Table 1. The systems simulated contained a total of ∼ 22000–28000 atoms. The lipid bilayer was oriented in the x-y plane, so z was the reaction coordinate for the permeation process. A constant temperature of 310 K was maintained with a Nose-Hoover thermostat (τ = 2 ps). The pressure of 1 bar was maintained by semiisotropic Parrinello-Rahman barostat (τ = 2 ps). Electrostatic interactions were calculated using the particle-mesh Ewald method with a Fourier spacing of 0.12. The cutoff distances for electrostatic and dispersive interactions were set to 1.4 nm.

The potential of mean force (PMF) was calculated using an umbrella sampling approach [45,46] for NF penetration through the DOPC bilayer with and without CLR, and in the presence and absence of GA. 39 or 20 windows spaced by 0.2 nm apart were used. In the case of models with a GA molecule, it was initially placed in the left half-layer and remained there for about 400 ns; therefore, the set of windows contained both left and right half layers, a total of 39 pieces. A harmonic restraining potential in the z-direction was applied to the center of mass of the NF molecule with a force constant of 800 kJ/mol/nm^2; the reference point was the bilayer midplane. The GA molecule could move freely. Each production run window contained 300–400 ns of simulation, covering a total of ∼ 42 μs. PMF reconstruction was performed using the weighted histogram analysis method [46,47], incorporated in GROMACS, with the periodic boundary conditions taken into account for the periodic PMF. 100 bins were used and the PMF zero point was set at −3.6 nm from the midplane where the water is bulk. The Supplementary material contains a convergence analysis of the resulting free energy profiles. The starting configurations for the umbrella sampling windows were generated via pulling simulation: the NF molecule was dragged through the membrane with the rate of 0.01 nm/ps along the z-axis, then the appropriate configurations were picked out as starting for further use in PMF calculation. Each window assumes a 100–250 ns pre-equilibration period that has been dropped. When calculating the PMF, the windows were symmetrized relative to the center of the bilayer. But the set of windows assumes that the initial position of the GA should be in the left half-layer of the bilayer (z < 0). And during the entire time of production runs, the GA molecule remains in the left half-layer in the case of DOPC without cholesterol. This is consistent with our previous results [28], where it was shown that the PMF profile for the penetration of the GA molecule through the DOPC bilayer has a potential barrier in the midplane with a height of about 5 kT, which reduces the probability of GA penetration into the second half-layer.

Calculations of hydrogen bonds, minimum distance, local density profile, and GA backbone angle were performed using standard GROMACS tools. The criterion for finding the H-bond was 30° for the O-H-O angle and 3.5 Å for the O-O distance.

2.5. Solubility-diffusion model

The effective membrane permeability P_{eff} was calculated similarly to previously published works [32] and a number of other works [37,48]. The method relies on the general diffusion theory of transport in the diffusional limit, where the average flow rate is proportional to the thermodynamic driving force [49]. Briefly, P_{eff} is inversely proportional to the integral of the local permeability resistivity $R(z)$ of each membrane slice, which can be expressed as the ratio of the mean force potential ΔG with a Boltzmann weight and the position-specific diffusion coefficient D:

$$1/P_{eff} = \int_0^Z R(z)dz = \int_0^Z \frac{e^{\Delta G(z)/kT}}{D(z)}dz \qquad (1)$$

Table 1
The composition of all systems used in the present work.

	System	NF	GA	DOPC	CLR	Water	Preliminary relaxation, ns	Runs/windows	Pproduction run, ns
PMF	NF + DOPC	1	–	128	–	6112	20 × 100	20	20 × 400 ns
	NF + GA + DOPC	1	1	128	–	5302	32 × 250	36	34 × 300 ns +
									1400 ns + 1400 ns
	NF + CLR + DOPC	1	–	114	14	7161	20 × 150	20	20 × 300
	NF + GA + CLR + DOPC	1	1	114	14	6756	39 × 100	39	37 × 300 s +
									1300 ns + 1300 ns
MD	NF + DOPC	1	–	128	–	7341	–	1	600
	NF + GA + DOPC	1	1	128	–	7341	–	1	600
	NF + 2GA + DOPC	1	2	128	–	10,087	–	4	4 × 600
	NF + 2GA	1	2	–	–	5575	–	1	250
	NF + CLR + DOPC	1	0	114	14	7108	–	1	600
	NF + GA + CLR + DOPC	1	1	114	14	7076	–	2	2 × 600

The diffusion coefficient profile was calculated according to Hummer [50] as:

$$D(z) = \frac{var(z)}{\tau_z} \qquad (2)$$

where $var(z) = \bar{z^2} - \bar{z}^2$ is the variance of the average reaction coordinate of the permeant and τ is the correlation time of damped oscillations for the permeant constrained by umbrella sampling.

3. Results and discussion

As mentioned above, two mechanisms are proposed for enhancement the bioavailability of NF in the complex with GA are suggested, namely, an increase in solubility and an increase in permeability. In the present study, we check both of these possibilities.

3.1. Solubility study

The solubility of nifedipine was studied experimentally by dissolving the free drug and mechanochemically prepared solid GA/NF mixture in water. The resulting solubility of GA/NF composition and unprocessed nifedipine is shown in Table 2.

We found that the solubility of the GA/NF complex in water is 35 times larger than that of free NF. It was previously demonstrated that this is due to an inclusion complex formation with GA micellar or pre-micellar aggregates [20]. The NF solubility enhancement, measured in [20] in 5% methanol solution, was approximately 10 times for pre-micellar GA aggregates, i.e., at GA concentrations below critical micelle concentration (cmc ∼ 1 mM for GA), and about 40 times for micellar solutions. Using the NMR technique (Job plot measurement), the stoichiometry of the inclusion complex was calculated as 2:1 GA/NF mole ratio at GA concentrations below critical micelle concentration [20]. It is known that the ability of GA to form self-associates (micelles) in aqueous solutions depends on the pH of the medium [24]. GA has three dissociation steps with pKa values of 3.98, 4.62 and 5.17. Recent results obtained by O. Yu. Selyutina with coauthors show that the GA/NF complex exists over a wide range of solution

pH [33]. In the present study, the solubility measurement was performed for a full protonated form of GA, the formation of stable associates of NF with the GA dimer was confirmed by MD simulation (see the next section "Unconstrained simulation of GA/NF complex").

3.2. In vitro parallel artificial membrane permeability assay (PAMPA)

In the present study, the influence of GA on the permeability of a model lipid membrane was studied by the PAMPA method using an artificial membrane composed of DOPC phospholipids. The plots (Fig. 2) clearly showed that the permeation of nifedipine across the artificial membrane is significantly enhanced in the GA/NF composition as compared to the pure nifedipine.

The results show a remarkable increase in the amount of nifedipine permeated in comparison with a saturated aqueous solution of pure drug used as control. The effect is dose-dependent. Note that all measurements were performed for a fully protonated form of GA at pH = 3.5. However, recent results show that GA/NF complex exists over a wide range of solution pH [33]. The enlargement of GA/NF concentration from 0.64 g/l (corresponds to 0.5 mM GA) to 6.4 g/l (corresponds to 5 mM GA) results in permeation enhancement from 27 mg (free NF) up to 85 µg respectively during 2.5 h. The obtained result is in agreement with the sharp increase in the bioavailability of nifedipine obtained in *in vivo* experiments. According to the data of Tolstikova et al. [11,12], the GA/NF complex with an active substance content 10 times less than pure NF showed antihypertensive efficacy similar to that of pure NF. It was concluded that the GA/NF composition

Table 2
The water solubility of NF and GA/NF composition.

	The improvement of solubility, times	The solubility of nifedipine, mg/l
Nifedipine	–	12.3
GA/Nifedipine (mole ratio 1/2, milling 2 h)	35	432
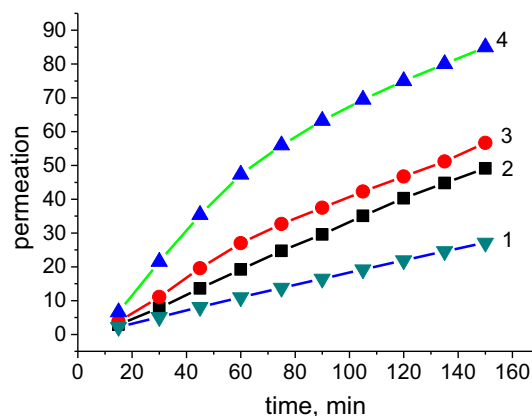
Fig. 2. The parallel artificial membrane permeability assay of nifedipine (saturated solution (1)) and its complex with GA. The concentration of GA is 0.5 mM (2), 1 mM (3), and 5 mM (4).

can be used for the prevention and treatment of acute arterial hypertension.

Using the known parameters of filter plates (12 mm diameter inserts, an area of 1.12 cm^2) and the volume of wells (1.5 mL of an acceptor plate and 0.5 mL of a donor plate), we can estimate the permeability of NF molecules through a model membrane (Eq. (3)).

$$P = V/(A \times C_0) \times dC/dt \tag{3}$$

Here P is the permeability in cm/s, V is the volume of the receiver compartment, A is the surface area, C_0 is the starting concentration in the donor compartment in mg/l, and dC/dt is the rate of change of compound concentration in mg/l in the receiver compartment. The resulted permeability of free NF is P = 3.6 ± 0.2 cm/sec. This value is the average over three measurements. The permeation rate (dC/dt) increases by the factors of 1.9, 2.6 and 4.3 at a GA concentration of 0.5, 1.0 and 5.0 mM.

Although the total solubility of NF increases in the complexes with GA: $[NF]_{total} = [NF]_{free} + [NF/GA]$, the concentration of free NF molecules in solution decreases according to Eq. (4).

$$K = [NF/GA]/([NF]_{free} \times [2GA]_{free}) \tag{4}$$

Here K is the stability (equilibrium) constant of the complex, $[NF/GA]$ is the concentration of NF in the complex, $[NF]_{free}$ is the concentration of free NF, and $[2GA]_{free}$ is the concentration of free GA dimers. Recall that, according to the data published, the NF/GA complex consists of one NF molecule and one GA dimer

(Fig. 2), and the stability constant of this complex is K = 1.2 × 10^5 M^{-1} [20]. Simple estimations give $[NF]_{free}$ = 1.4 μM at 0.5 mM of GA and ∼ 5 μM at 5 mM of GA. These values significantly reduce the solubility of the uncomplexed drug (33 μM) measured in the present study. Thus, it can be concluded that almost all NF molecules are in complexes with GA molecules in aqueous solution.

3.3. Unconstrained simulation of GA/NF complex

MD simulations can help to study the structure of the GA/NF complex in water, as well as its landing on the membrane and its entrance. We studied a single NF molecule that landed on both pure DOPC bilayer and DOPC with cholesterol, as well as host–guest complexes in a 1:1 and 2:1 ratio with GA.

We first examined the behavior of the free NF molecule and the GA/NF complex near the pure DOPC lipid bilayer and DOPC with cholesterol (CLR). Simulations show that after a short interval of free diffusion in water, the NF molecule settles on the membrane and moves along the surface for about 10–150 ns (Fig. 3 b). When walking over the bilayer surface, NF (or GA/NF complex) finds a cavity suitable for insertion and then penetrates into the bilayer. After penetration into the DOPC bilayer, the NF remains there for at least 500 ns and does not pass into the next half-layer during the simulation period. In one of the following sections on free energy calculation, it will be shown that there is an energy barrier in the midplane of the membrane. Snapshots of all the stages described here can be found in the Supplementary Material, Figure S1 - Figure S4.
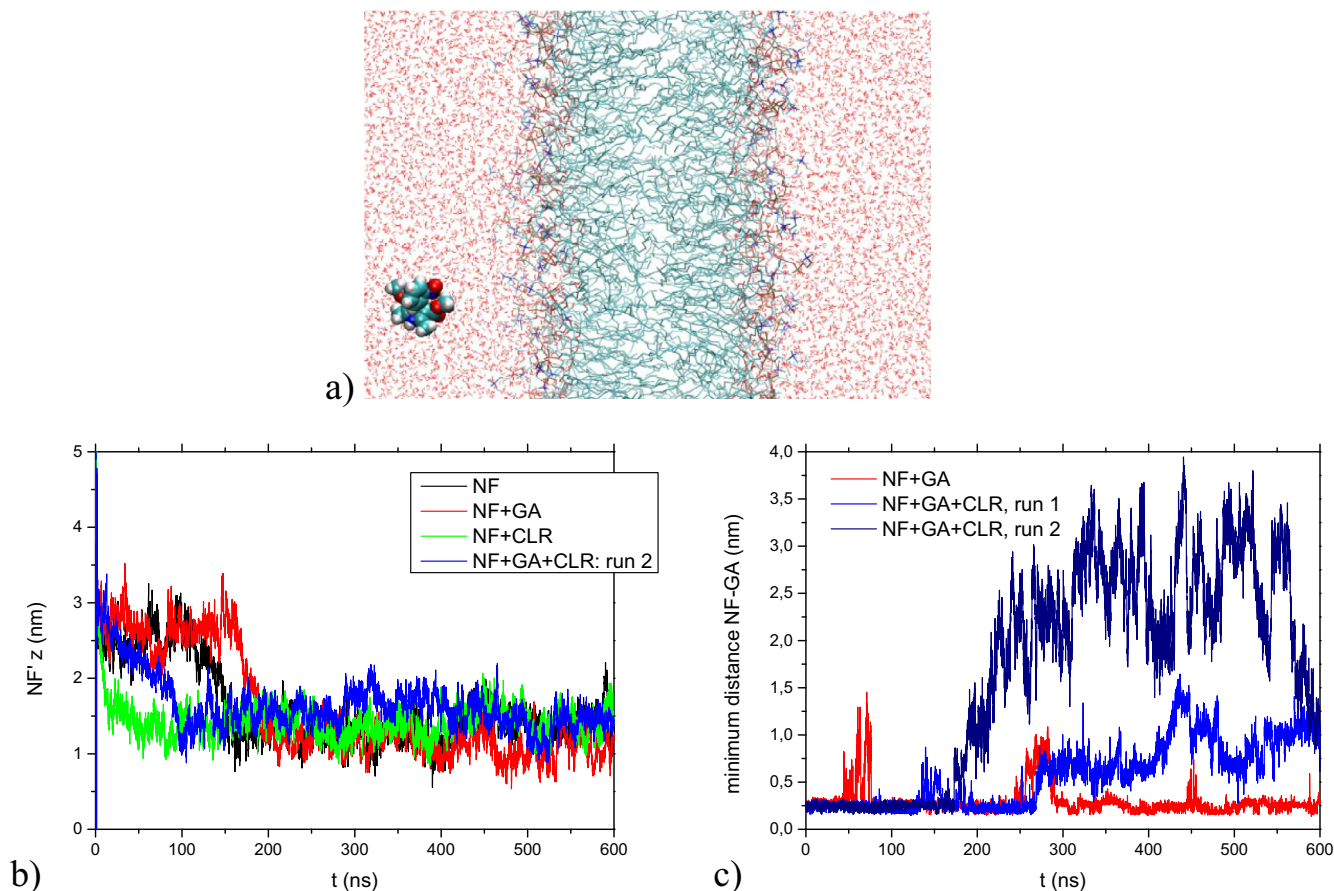
Fig. 3. a) The starting configuration for NF simulation in the vicinity of the DOPC lipid bilayer. DOPC and water molecules are shown by lines, NF - by VDW spheres. b) z-position of the NF molecule relative to the center of the DOPC bilayer for: 1) NF near pure DOPC (black), 2) NF and GA complex near pure DOPC (red), 3) NF near DOPC with CLR (green) and 4) NF and GA complex next to DOPC with CLR (blue). c) Minimum distance between NF and GA in the pure DOPC membrane (red) and DOPC + CLR for two runs, shown in blue and dark blue. In the "dark blue" case, the GA molecule passed into the next half-layer and remained there until the end of the simulation.

The GA/NF complex can disintegrate and reunite, as happened once on the surface of pure DOPC, and another time inside the bilayer (Fig. 3 c, red line). But when the membrane contained the CLR molecules, the GA/NF complex fell apart (Fig. 3 c, blue and navy lines), and in another run, the GA molecule moved to the next half-layer, and the distance to NF increased even more (Fig. 3 c, navy lines).

We also performed MD simulation of 2 GA and one NF molecule in water. As we mentioned above, such a stoichiometry was taken from experiments on the complexation of the GA with NF at low GA concentrations. MD simulations demonstrate the formation of the stable complex that does not fall apart during a simulation of 250 ns. The complex is flexible; its conformations can be classified into 3 types: Fig. 4 a, b and c, where two GA molecules can be crossed (a, b) or collinear (c) when the guest NF molecule occupies the pocket formed by sucrose rings (a) or terpene tails (b).

Several MD simulations were performed to study the penetration of the 2:1 complex into the DOPC bilayer. The starting configuration is shown in Fig. 5 a: the pre-equilibrated complex was placed in water near the DOPC bilayer. We observed the complex as stable not only in water and near the bilayer, but also upon penetration into the membrane (Fig. 5 b). However, inside the bilayer, the complex falls apart (Fig. 5 c). In all of these runs, the NF molecule did not pass to the next half-layer during the simulation run.

To study the dynamics of penetration, the minimum distance between the atoms of the complex and the terminal C atoms of DOPC lipids were calculated. We also computed the minimum distance between the atoms of the NF and GA molecules to study the integrity of the complex. Four independent MD runs of 600 ns long were performed. Fig. 6 shows the time dependence of the minimal distances between the complex and the DOPC membrane (black line) and between the molecules of nifedipine and GA (blue line).
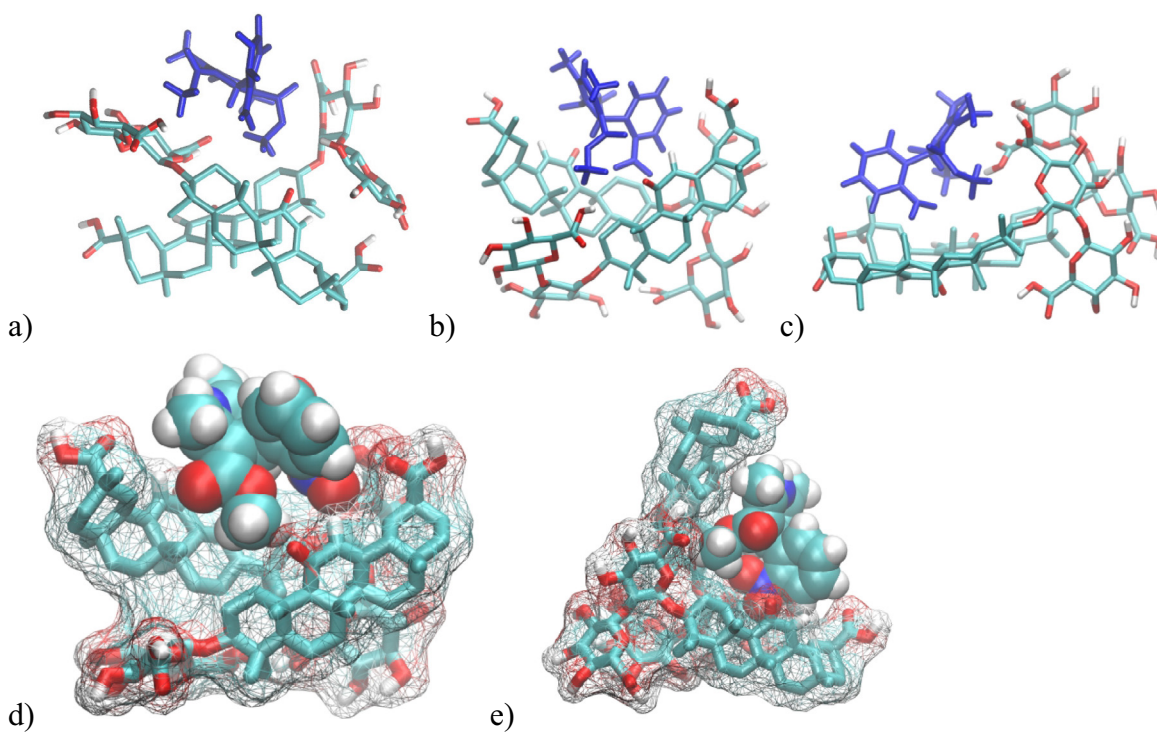
Fig. 4. a), b), c) the simulated GA/NF complexes in a 2:1 ratio obtained in this work, 3 types of complexes: d), e) - the surface of the GA dimer is shown as a wireframe, so the pocket for the guest molecule of GA can be seen.
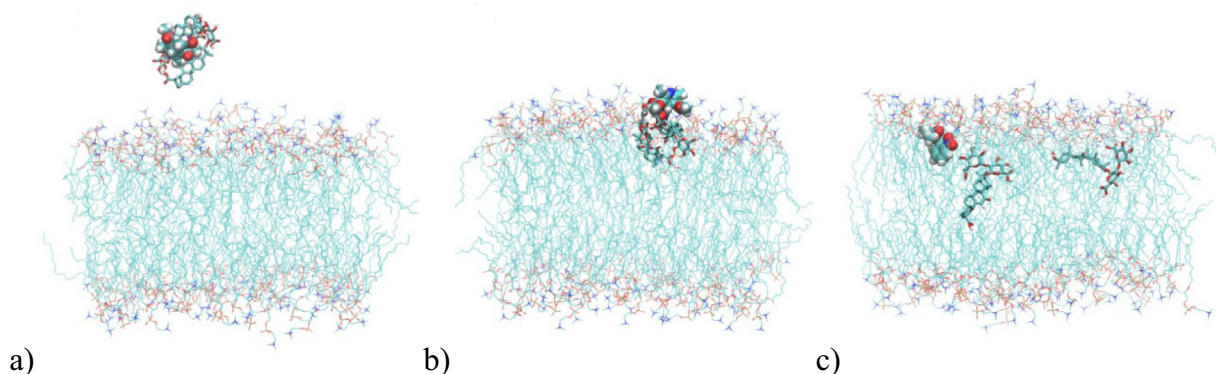
Fig. 5. Penetration of the GA/NF complex 2:1 inside the DOPC bilayer. a) initial configuration, b) penetration, c) the complex fell apart inside the bilayer. The nifedipine molecule is shown with its van der Waals radii; GA molecules are shown in bold lines. Water molecules are not shown for clarity.
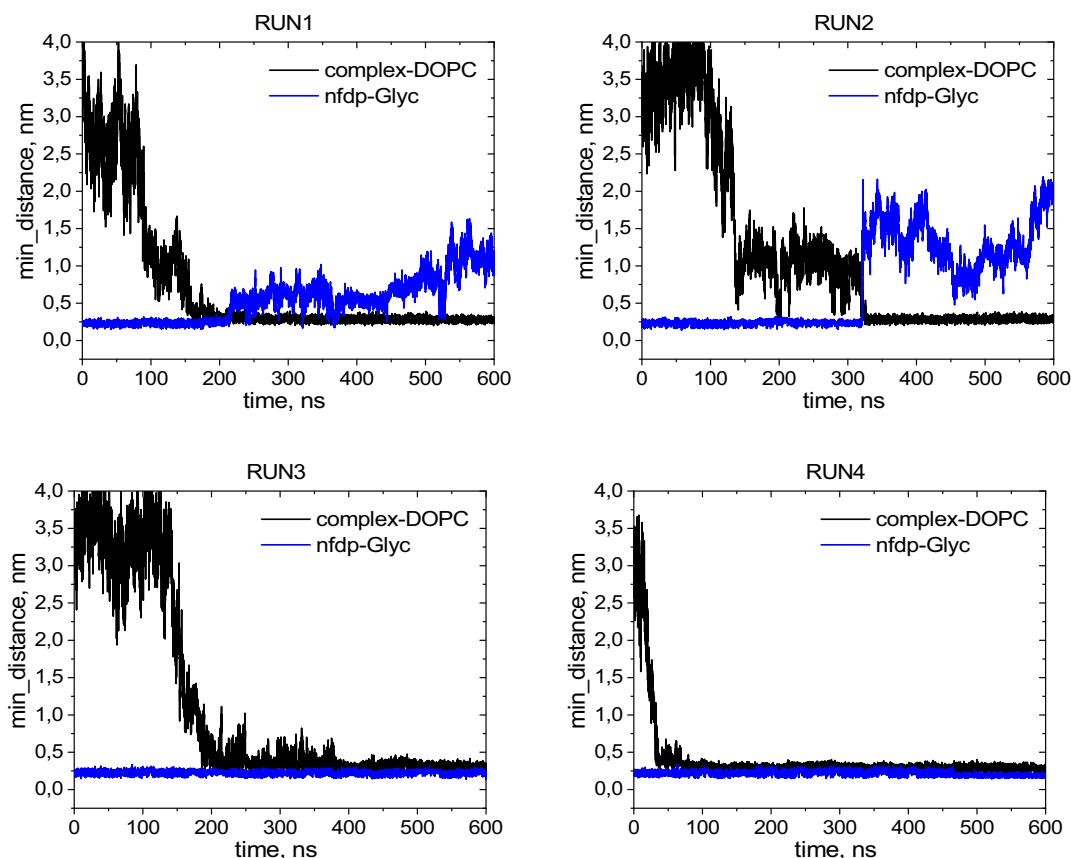
Fig. 6. Time dependence of the minimum distances between the complex and the terminal C atoms of DOPC lipids (black line), and between the nifedipine and GA molecules (blue line) for four independent runs.

As can be seen, the GA/NF complex approaches the bilayer surface in 50–200 ns, settles on the surface for some time, and then moves inside the bilayer. The distance between the molecules of the complex shows that it remains whole in water and on the bilayer surface. Note that the average penetration time observed (∼300 ns) is much longer compared to individual molecules that penetrate the bilayer in tens of ns [28]. However, we cannot judge from several MD runs for each model whether the observed behavior is typical or not - only the calculation of the free energy can give us an answer to this question. But in any case, the classical MD is useful in that it gives examples of the NF penetration into the bilayer.

So, our results show that GA helps nifedipine reach the bilayer surface by increasing its water solubility. In practice, GA and NF are dissolved in water together as an inclusion complex with a GA dimer or micelle as a drug carrier, but it is known that the inclusion complex in solution exists in equilibrium with free molecules; therefore, NF and GA can enter the bilayer separately. Next, we consider a bilayer that already contains a GA molecule and investigate its NF permeability compared to a pure bilayer.

3.4. Free energy calculation of glycyrrhizin assisted NF transport through the membrane

To study the process of NF penetration, we used a restrained MD. We generated a set of the full-atomistic molecular dynamic simulation runs of the DOPC lipid bilayer and calculated the potential of mean force (PMF) for a nifedipine molecule to penetrate the bilayer in the presence and absence of GA. Since we have observed

that the GA/NF complexes fall apart inside the membrane, here we calculate the PMF for a free NF molecule.

3.5. Free energy profile

Fig. 7 a) shows a typical view of the DOPC model membrane for PMF calculation: the GA molecule is located just below the surface of the lipid bilayer. The z-axis zero is placed at the midplane of the bilayer. The NF molecule is constrained in the z-position and can move freely in the x,y-plane. Fig. 7 b) shows the potential of mean force for the nifedipine penetration through a pure DOPC bilayer and a bilayer with one GA molecule embedded. The profile was symmetrized around zero. Error bars come from the standard WHAM calculation. The PMF convergence analysis can be found in Supplementary materials Figure S5- Figure S9; convergence was achieved at 260–300 ns of production runs.

For all the systems, there is a potential well just below the surface and a potential barrier in the midplane of the bilayer. In the absence of a GA (Fig. 7 b, dashed lines red and blue) the midplane barrier reaches a value of about −2 kCal/mol. Also, in the presence of cholesterol, the barrier is wider (Fig. 7 b, dashed blue line), and the well is not as deep as for pure DOPC. The addition of the GA molecule to the membrane lowers the midplane barrier to −4 kCal/mol (Fig. 7 b, solid lines) and makes the presence and absence of CLR similar (Fig. 7 b, solid blue and red lines, respectively), the barrier becomes less wide and similar to that one for pure DOPC. Thus, the GA molecule cancels the effect of cholesterol on the DOPC bilayer, which consists in shallowing subsurface pits and widening the midplane barrier for NF penetration through the bilayer.

a)

b)

c)

d)
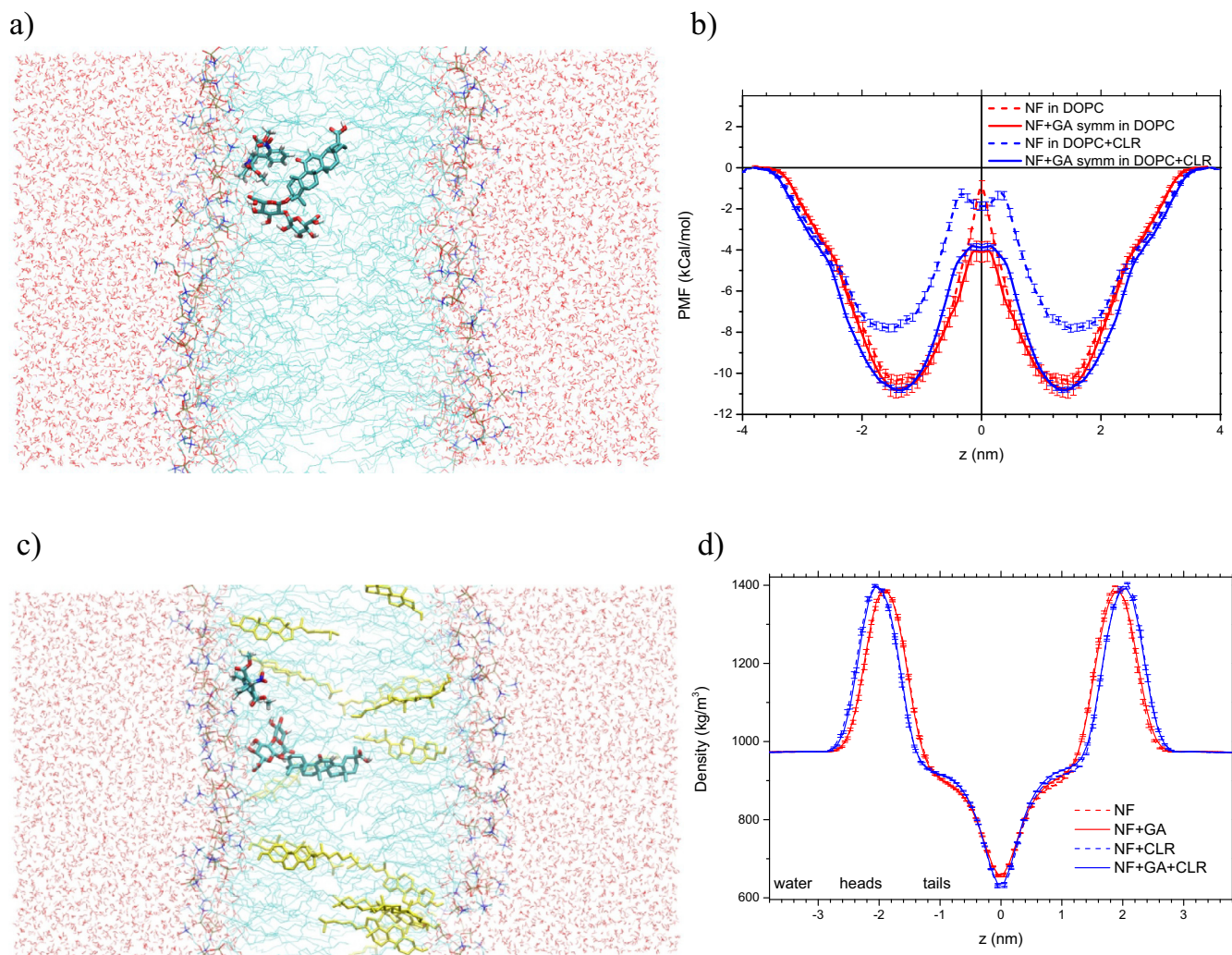
Fig. 7. a) A typical view of the DOPC membrane for PMF calculation. b) symmetrized free energy profiles for the penetration of NF through the lipid bilayer (dashed lines) and the membrane with the GA molecule (solid line). The blue and red colors of the lines correspond to the DOPC bilayer with and without cholesterol, respectively. c) the same as a), but with cholesterol in the membrane. d) Local density profile of all four systems; enlarged portions of the profile can be found in Figure S10.

The local density profiles (Fig. 7 d) show the densification of the lipid head regions, which is determined by the location of heavy phosphorus atoms. For further convenience in describing the position of the NF molecule in the membrane, we conditionally divided the z-axis into several regions: "water", "heads", "tails", and "zero" in the middle of the bilayer.

3.6. Analysis of the impact of GA

3.6.1. Hydrogen bonds

We hypothesized that the mechanism for decreasing the midplane barrier may involve the H-bond interaction between GA and NF molecules. Indeed, the profiles of the H-bonds number between NF and GA molecules (Fig. 8, red diamonds) show a peak around z = 0. The NF molecule can form up to 6H-bonds. But in the middle of the membrane, no polar groups can access the NF molecule. In this situation, the GA molecule comes to the rescue of the NF molecule and forms with it one H-bond on average. Examples of H-bonds are shown in Fig. 8c–e. The hydrogen bond profiles for membranes with and without CLR are almost the same. The total number of NF's H-bonds can be found in Figure S11.

3.6.2. Membrane thickness and area per lipid

The membrane becomes thicker with the addition of CLR (Fig. 9 a); this is generally believed to be due to the ordering effect of CLR on lipid tails, see the order parameters in Figure S13. The addition of the GA or NF molecules does not change the membrane thickness (Fig. 9 a), but increases the area per lipid (Fig. 9 b) especially in the absence of CLR. The area per lipid was calculated as the area of the membrane plane divided by the amount of lipids in the half-layer. In pure DOPC (Fig. 9 b, green), the area per lipid is the smallest of the four systems, and the addition of the GA molecule increases the area to the maximum of all systems (Fig. 9, yellow). The presence of NF is also seen in the bell-shaped profile of the area per lipid (Fig. 9 b). The question arrives, why does GA increase the area per lipid in the presence of CLR not as much as in the absence (Fig. 9 b)? The answer is in its orientation. In the case of DOPC without CLR, the GA molecule is oriented parallel to the membrane surface (Fig. 13a, Figure S16 a, c, e) and loosens lipid molecules, so the membrane expands. But in the presence of CLR, the GA molecule is oriented predominantly perpendicular to the membrane (Fig. 13b, Figure S16 b, d, f) and straightens the lipids, causing the membrane to contract. In pure DOPC, the order parameter of lipid molecules surrounding GA is 9% lower than in distant
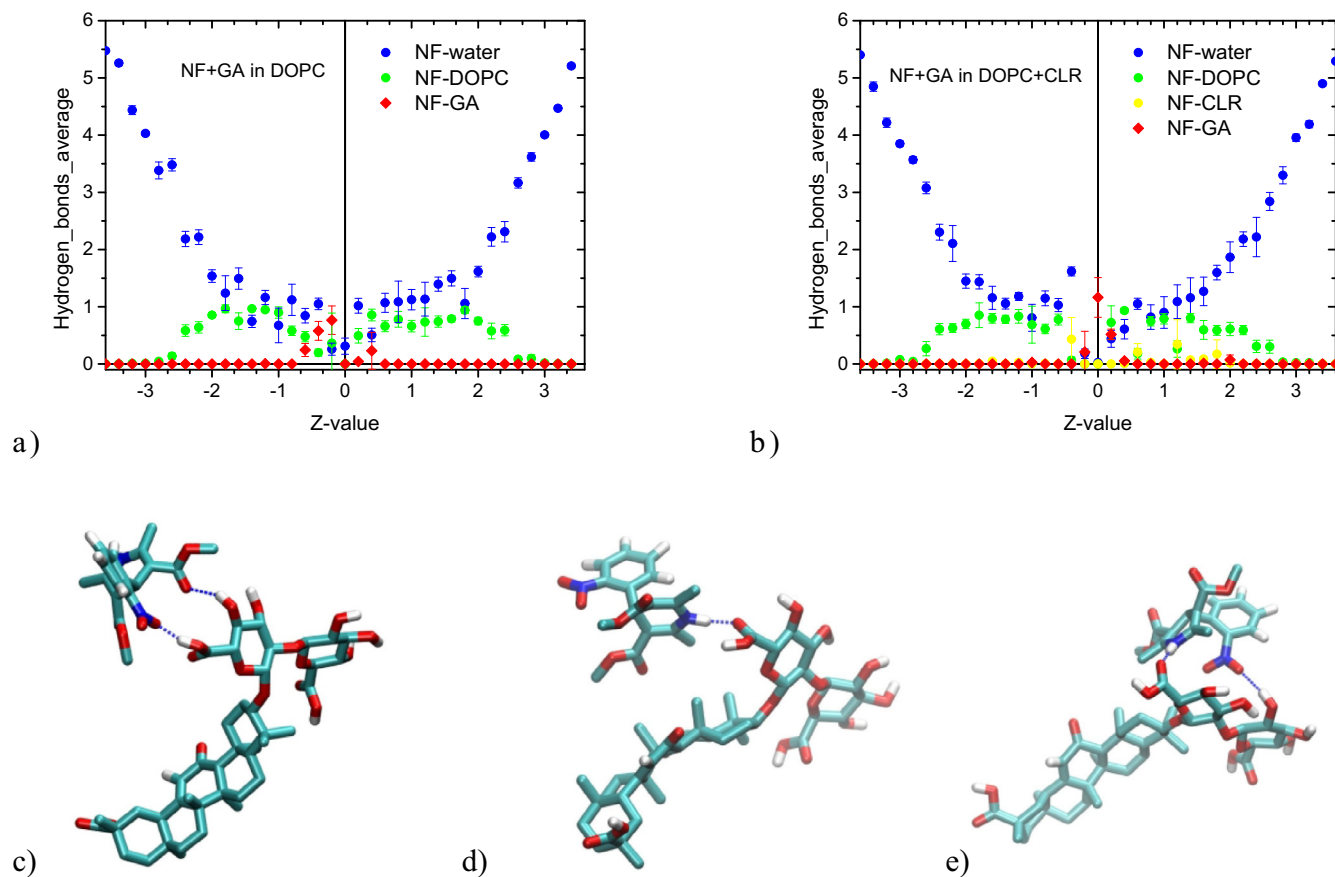
Fig. 8. Profiles of the number of hydrogen bonds of the NF molecule with water molecules (blue circles), DOPC atoms (green squares), and GA molecule (red diamonds) in the systems: a) DOPC + GA membrane, b) DOPC + CLR + GA membrane. A set of simulations for PMF calculating was used as a data source, so the abscissa z corresponds to the position of the NF in the membrane. The left half-layer (z < 0) contains the GA molecule. c), d), e) - examples of H-bonds between GA and NF molecules from the DOPC + GA system; examples from the system with CLR are almost the same and are shown in Figure S12.
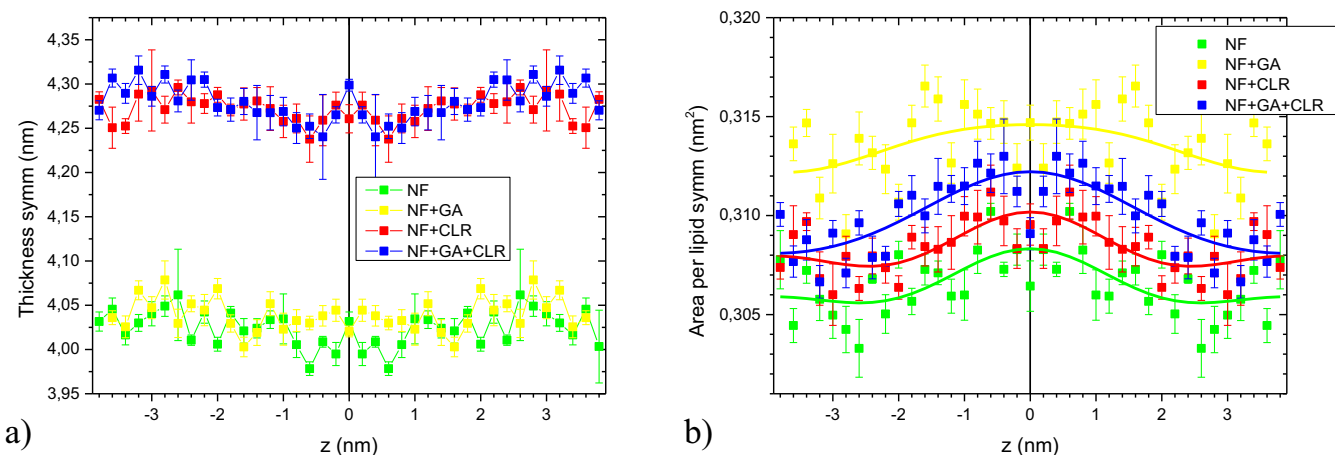
Fig. 9. a) The thickness of the membrane for all 4 systems depending on the location of the NF molecule (umbrella windows); b) the area per lipid. A system with pure DOPC is shown in yellow, DOPC with GA in green, DOPC with CLR only in red, and DOPC with CLR and GA in blue. Both plots are symmetrized around z = 0.

lipids (Fig. 10) or lipids from the models without GA. The membrane with CLR is compacted to such an extent that the addition of a small NF molecule causes the membrane to enlarge, Fig. 9 b, red, z ∈ (-2; 2).

3.6.3. Order parameters

To characterize the effect of GA on the ordering of lipid tails, the order parameter was calculated for several distances between the centers of mass of the GA molecule and lipid molecules. Fig. 10
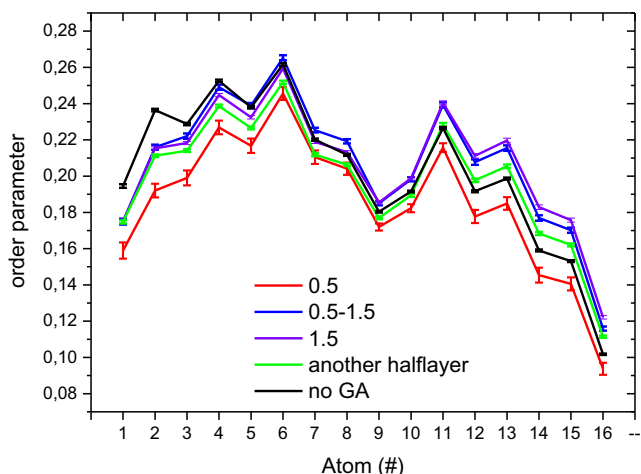
Fig. 10. DOPC order parameter of lipids around GA for the distances between GA and the center of mass of the lipid molecule: < 0.5 nm (red), 0.5–1.5 nm (violet), lipids from another half-layer relative to GA (green) and for the model of the pure lipid bilayer.

Fig. 12. Selection of the GA backbone vector.

shows that lipid tails are disordered in the immediate environment of GA at a distance of <0.5 nm apart and become more ordered over large distances. This is in agreement with our previous work, where we showed that the GA molecule, located in the membrane with cholesterol, has an ordering and condensing effect on the nearest lipids, straightening and locally densifying them [51].

3.6.4. Minimum distance NF-GA

In our set of windows, the NF molecule is constrained in the middle of each window in the z-direction, but the GA molecule is free to move. To inspect this behavior, we calculated the minimum distance between GA and NF molecules for each window - the resulting population diagram is shown in Fig. 11. Another representation of the same data is in Figure S14, where the minimum distance is a function of time for different z-windows. The minimum distance connects the nearest atoms of GA and NF in the current frame. The diagram shows that GA prefers to be close to the NF molecule when it is constrained in the midplane of the membrane, so the minimum distance is 0 at z = 0. The GA molecule provides NF a possibility to form H-bonds when it is located in an

energetically unfavorable midplane of the membrane (see Fig. 7). In the case of a CLR membrane, the midplane barrier is wider (Fig. 7), so the zero-region is wider in Fig. 11 b.

When the NF molecule is constrained not in the middle of the membrane, this does not force the GA molecule to be adjacent to the NF, so GA moves along the entire xy-plane. The graph shows that the minimum distance increases with a slope of ± 1. This slope is trivial if we understand that the GA molecule occupies mainly a groove in the left half layer, and NF is held alternately in each z-window. It can be seen that in pure DOPC, GA and NF molecules aggregate only in the middle of the bilayer (Fig. 11 a). But in the CLR + DOPC bilayer the GA molecule prefers to be next to the NF molecule on the entire left side of the DOPC + CLR membrane (Fig. 11 b). This can be explained by the disruption that GA introduces into the lipid tails of the cholesterol-containing membrane DOPC, which is more densely packed than pure DOPC, so it is more difficult for NF to pass it - see the potential well in Fig. 7 b shown with a blue dashed line - it is shallower than in pure DOPC, red dashed line. But adding GA significantly deepens the potential well in the case of CLR + DOPC (blue dashed → blue solid line). Here, in some windows, a lack of sampling was revealed, which is reflected in the spotty organization of the diagrams Fig. 11.

3.6.5. Angle-position diagrams of the GA molecule

To understand the peculiarities of not only position, but also the orientation of GA in the DOPC membrane, we set the angle between the GA backbone (Fig. 12) and the normal to the nearest surface of the membrane.

This angle was examined, as well as the position of the GA's center of mass relative to the center of the membrane in the z
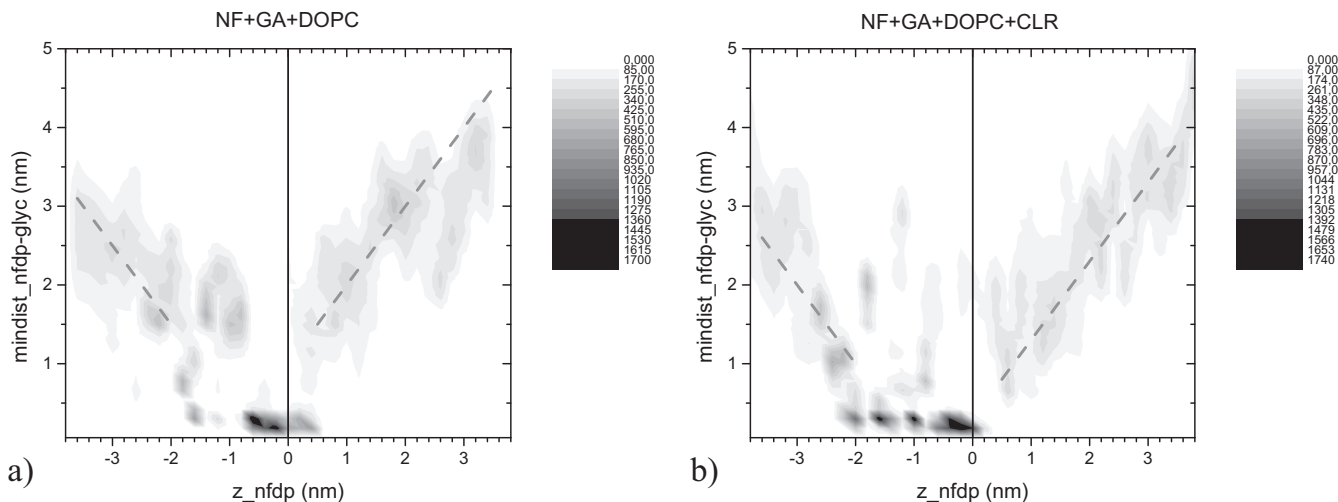
Fig. 11. The minimum distance between GA and NF depending on the NF position in a) DOPC, b) DOPC with CLR. The darkness indicates the population of such a minimum distance. The GA molecule moves freely in the left half of the membrane (z < 0). The dashed lines have a slope of ± 1.
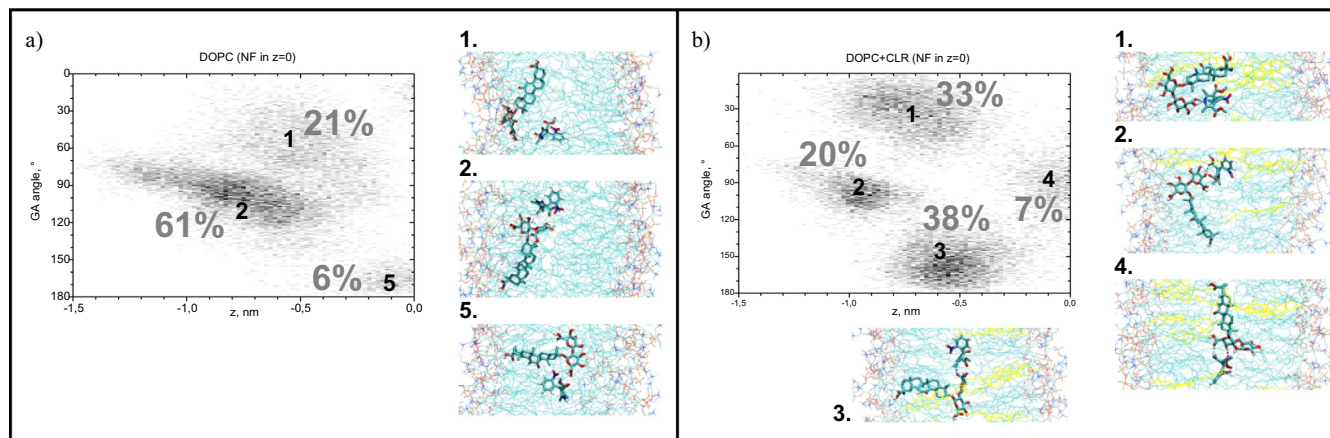
Fig. 13. The population of the angle-position diagrams of the GA molecule: ordinate axis - the angle of the GA backbone and the normal to the closest membrane surface and abscissa axis - the position of the GA center of mass (COM). The NF molecule is constrained in the middle of the membrane. Columns a) and b) correspond to the pure DOPC membrane and DOPC + CLR, respectively. The states observed in the diagrams are numbered, and typical examples of the corresponding configurations are shown next to the diagrams (CLR molecules are colored yellow, water molecules are not shown). The membrane without CLR (column a) contains the GA molecule oriented parallel to the membrane surface, and in the membrane with CLR (column b) the GA is perpendicular to the surface.

direction. The population diagram of the angle and position of the GA molecule is shown in Fig. 13 - here the NF molecule was constrained in the middle of the membrane in the z direction. There are several preferred states - the corresponding spots are numbered and typical snapshot examples are shown. The right and left panels refer to DOPC membranes with and without CLR, respectively. In the case of pure DOPC, the GA molecule prefers to orient itself mainly parallel to the membrane (state 2), while in the membrane with CLR it is oriented mainly perpendicular to the surface (states 1 and 3). This difference can be explained by the ordering effect of the CLR, which orients not only lipid tails, but also the GA backbone. It should be noted that for the more representative ensembles, the sampling was increased up to 1400 and 1300 ns for both the models of DOPC with a and without CLR (the window z = 0.0). A similar analysis was performed for cases where NF is constrained in water, lipid heads and lipid tails (see Figure S16).

3.7. Diffusion coefficient profile

The diffusion coefficient profiles calculated by the Hammer method (formula 2) are shown in Fig. 14. Autocorrelation time and variance profiles can be found in Supporting Information (Figure S17, Figure S18); they are very similar to the results of our previous study of praziquantel [32]. The D values inside the membrane are an order of magnitude lower than in water, which is evident, since the lipid bilayer has a higher density. A slight increase of D in the midplane corresponds to a rarefaction of the medium between the lipid tails. At z = ±3.8, where the water is almost bulk, the D values calculated by the Hammer method are close to the D obtained from the mean square deviation of NF lateral diffusion, also shown in Fig. 14.

3.8. Permeability

The local resistivity profile $R(z)$ (Fig. 15 a), calculated as a combination of the free energy and diffusion coefficient profiles (formula 1), shows that the main contribution to the resistance is made by the mid-plane barrier and the interfacial region in different ratios. The resistance to penetration of NF through DOPC heads and most of its tails is negligible compared to water. But the midplane barrier in free energy dictates a high resistance in this region for pure DOPC membrane and membrane with CLR. Although the diffusion rate of NF in the membrane is low, the shape of the per-
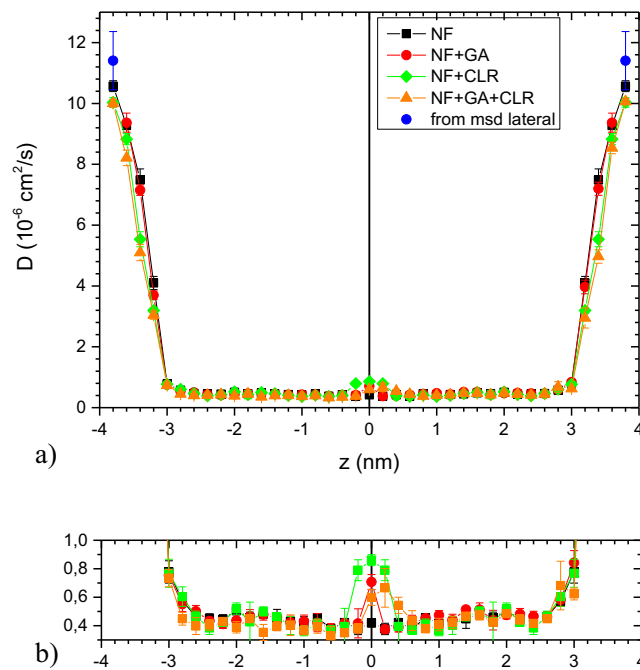
Fig. 14. Diffusion coefficient profile of NF penetration through the pure DOPC lipid bilayer without GA (black squares) and with GA (red circles), DOPC + CLR without GA (green rhombs) and with (orange triangles). a) - full scale, b) - enlarged scale. D values calculated from the mean square deviation of NF lateral diffusion at z = ±3.8 nm are shown with blue circles.

meation resistance profile is primarily determined by the free energy, since it has a Boltzmann weight (see the same data on a logarithmic scale in Figure S19). The addition of GA in both pure DOPC and DOPC with CLR reduces the resistance of the midplane by a factor of 100 and allows NF to flow from the left to the right water compartment. Surface resistivity also decreases in the presence of GA (Fig. 15 b), which can also be explained energetically or by rarefaction of the lipid heads.

Since the water medium has nonzero resistivity to NF penetration, the value of the effective permeability depends on the boundaries of integration in formula 1. Fig. 16 shows these values of such accumulated permeability as a function of the second boundary Z. Integration starts from the bulk water at z = -3.8. At the exit from
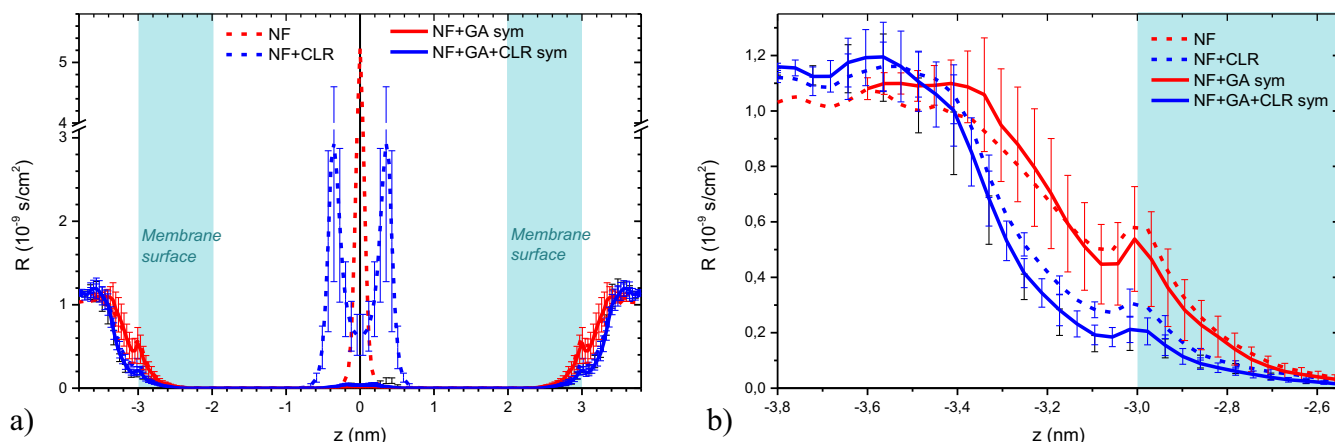
Fig. 15. a) Local resistance to penetration of NF through pure DOPC (red) and DOPC with CLR (blue) in the absence of GA (dashed lines) and in the presence (solid). b) Resistivity of the surface in more detail.
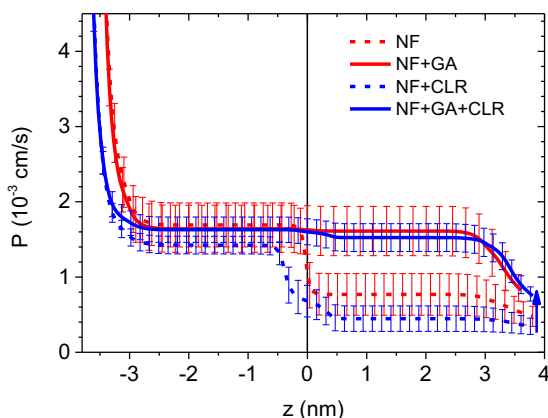
Fig. 16. Accumulated permeability of NF through the membrane.

the bilayer at $z = 3.8$, the NF molecule has a permeability value of $P = 0.48 \pm 0.13 \cdot 10^{-3}$ cm/s for pure DOPC without GA, and with GA it is doubled $P = 0.82 \pm 0.17 \cdot 10^{-3}$ cm/s. Similarly, for the membrane with CLR but without GA, the permeability is $P = 0.34 \pm 0.1 \cdot 10^{-3}$ cm/s, and in the presence of GA it becomes twice as large: $P = 0.75 \pm 0.09 \cdot 10^{-3}$ cm/s. The main contribution to the increase in permeability with the addition of GA is made mainly by the middle part of the membrane.

The source of errors in our free energy calculations can be the slow processes such as the migration of the GA molecule from one half-layer to another, which occurs approximately every 300 ns. Also, the GA molecule could induce a phase transition of the lipid bilayer from a disordered state to a partially ordered one. Another slow process is the CLR migration from one half-layer to another, which we observed in our simulations (see Supplementary). There have also been rare cases of diffusion of water molecules through the bilayer. The limited size of the model can also limit fluctuations in membrane density or curvature.

As for the ordering of lipid molecules, cholesterol and GA have the opposite effect: CLR orders, and GA disorders, which is observed in experiments on lipid mobility and relaxation time.

From a common point of view [52], when we use surfactants to solubilize hydrophobic drugs, it is obvious that above the critical micelle concentration NF can be incorporated into surfactant micelles, which increases their solubility in water. However, micellar solubilization also leads to a decrease in the fraction of free

drug. Thus, the incorporation of the drug into micelles will reduce the amount of free drug available for the membrane permeation due to the lower concentration gradient.

Since we observed a significant increase in the incorporation time even for a small GA/NF complex, we believe that large glycyrrhizin complexes (in the micellar or premicellar state are larger than the dimer) cannot be incorporated into the lipid bilayer. Taking into account that, at a concentration of more than 1 mM (critical micelle concentration for GA) most GA molecules exist in micellar form, it can be concluded that the experimentally observed increase in the permeation rate at 5 mM of GA cannot be due to the solubilization of NF by GA micelles.

These results are important for understanding the mechanism of increasing the drug bioavailability in the presence of glycyrrhizin. First of all, GA forms non-covalent associates with hydrophobic drugs, which leads to an increase in their solubility and stability. Both the free NF molecule and the NF/GA complex can enter the lipid membrane. However, the increase in solubility (up to 33 μM at 1 mM of GA) is insufficient to explain the observed effects in the PAMPA experiment. According to some published results for various delivery systems, GA increases the solubility of tebuconazole (TBK) 3 times more effective than the disodium salt of GA, but the increase in the rate of penetration from the TBK/Na$_2$GA composition is even more effective [13]. That is why in the present study we proposed and tested an alternative mechanism for enhancing penetration, namely the interaction of the carrier with the membrane following the alternation of the membrane properties. MD simulations of the interaction of lipid bilayer with one, two, three or four GA molecules carried out in [28,31] shows that all GA associates have high adhesion to the membrane surface. However, only GA monomers and sometimes dimers can penetrate into the bilayer (Fig. 5). In addition, free GA molecules that have penetrated into the membrane can alter the membrane permeability by decreasing the energy barrier to drug penetration. This leads to increased penetration of nifedipine through the lipid bilayer.

4. Conclusion

PAMPA experiments and solubility studies show that GA increases both the solubility and the permeation rate of NF. An approximately 5-fold increase in the permeation rate and a 35-fold increase in the solubility of NF were obtained. The molecular mechanism of the increase in permeability was elucidated using MD simulation. We investigated two possible mechanisms for increasing the bioavailability of NF in the presence of GA, namely:

1) increasing the solubility of NF in water and 2) improving the membrane permeability for NF due to the membrane-modifying activity of GA. The MD simulation data demonstrate the presence of stable GA/NF complexes in water. It has also been demonstrated that GA/NF complexes are able to penetrate the bilayer without preliminary dissociation. Free energy calculations showed an increase in the DOPC membrane permeability for the NF molecule in the presence of GA. A barrier was found in the middle of the bilayer with a height of about 10 kJ/mol, which prevents the penetration of the nifedipine molecule through the bilayer. The ability of the GA molecule to lower the midpoint barrier to 5 kJ/mol may be associated with the H-bond interaction between GA and NF molecules in the middle of the bilayer. The presence of cholesterol influences the orientation of GA molecules in the membrane but does not affect the permeability increase. Thus, in the membrane with cholesterol, we also observed a decrease in the midplane barrier in the presence of GA, and the total permeability increased.

The CLR, in addition to thickening the lipid bilayer and ordering the lipid tails, preferentially orients the GA molecule backbone along with the CLR (perpendicular to the membrane). That's why the addition of the GA molecule does not thicken the lipid bilayer, but significantly increases its area in the absence of CLR and hardly increases in its presence.

The result corresponds to a sharp increase in the bioavailability of nifedipine obtained in previous experiments *in vivo*. The use of nifedipine in the form of the NF/GA complex allows the therapeutic dose to be reduced up to 10 times while maintaining the same antihypertensive efficacy as pure NF. It can be concluded that the NF/GA composition can be considered for the prevention and treatment of acute arterial hypertension. In conclusion, we believe that these results may shed light on the mechanism for the drug bioavailability enhancement in the presence of glycyrrhizin.

Declaration of Competing Interest

The authors declare that they have no known competing financial interests or personal relationships that could have appeared to influence the work reported in this paper.

Acknowledgements

References

[1] C. Bailly, G. Vergoten, Glycyrrhizin: An alternative drug for the treatment of COVID-19 infection and the associated respiratory syndrome?, Pharmacol Therapeut. 214 (2020) 107618, https://doi.org/10.1016/j.pharmthera.2020.107618.

[2] A. Lopalco, N. Denora, Nanoformulations for Drug Delivery: Safety, Toxicity, and Efficacy, Meth. Mol. Biol. 1800 (2018) 347–365, https://doi.org/10.1007/978-1-4939-7899-1_17.

[3] R.K. Tekade, R. Maheshwari, M. Tekade, in: Biopolymer-Based Composites, Elsevier, 2017, pp. 81–106, https://doi.org/10.1016/B978-0-08-101914-6.00004-1.

[5] A.V. Dushkin, T.G. Tolstikova, M.V. Khvostov, G.A. Tolstikov, Complexes of polysaccharides and glycyrrhizic acid with drug molecules. Mechanochemical synthesis and pharmacological activity, in: D.N. Karunaratne (Ed.), The Complex World of Polysaccharides, InTech, RijdrugCroatia, 2012, pp. 573–602, https://doi.org/10.5772/48182.

[6] A. Kumari, S.K. Yadav, S.C. Yadav, Biodegradable polymeric nanoparticles based drug delivery systems, Colloids Surf. B 75 (1) (2010) 849–862, https://doi.org/10.1016/j.colsurfb.2009.09.001.

[7] S. Shibata, A drug over the millennia: Pharmacognosy, chemistry, and pharmacology of licorice, Yakugaku Zasshi – J. Pharm. Soc. Japan 120 (10) (2000) 849–862, https://doi.org/10.1248/yakushi1947.120.10_849.

[8] O.Y. Selyutina, N.E. Polyakov, Glycyrrhizic acid as a multifunctional drug carrier – from physicochemical properties to biomedical applications: a modern insight on the ancient drug, Int. J. Pharm. 559 (2019) 271–279, https://doi.org/10.1016/j.ijpharm.2019.01.047.

[9] N.E. Polyakov, T.V. Leshina, Glycyrrhizic acid as a novel drug delivery vector, Synergy of drug transport and efficacy, Open Conf Proc. J. 2 (2011) 64–72, https://doi.org/10.2174/2210289201102010064.

[10] X. Su, L. Wu, M. Hu, W. Dong, M. Xu, P. Zhang, Glycyrrhizic acid: A promising carrier material for anticancer therapy, Biomed. Pharmacother. 95 (2017) 670–678, https://doi.org/10.1016/j.biopha.2017.08.123.

[11] T.G. Tolstikova, M.V. Khvostov, A.O. Bryzgalov, The complexes of drugs with carbohydrate-containing plant metabolites as pharmacologically promising agents, Mini-Rev. Med. Chem. 9 (2009) 1317–1328, https://doi.org/10.2174/138955709789878123.

[12] T.G. Tolstikova, I.V. Sorokina, A.O. Brisgalov, M.P. Dolgich, G.I. Lifshitz, M.V. Chvostov, The use of a new approach to prevention and therapy of acute arterial hypertension with complex of well-known drugs with vegetable glycosides (experimental study), Rational Pharmacother. Card. 1 (2006) 55–58, https://doi.org/10.20996/1819-6446-2006-2-1-55-58.

[13] K. Singh, A.M. Zaw, R. Sekar, A. Palak, A.A. Allam, J. Ajarem, B.K.C. Chow, Glycyrrhizic Acid Reduces Heart Rate and Blood Pressure by a Dual Mechanism, Molecules 21 (2016) 1291, https://doi.org/10.3390/molecules21101291. doi:10.3390/molecules26051270.

[14] E.S. Meteleva, Y.S. Chistyachenko, L.P. Suntsova, M.V. Khvostov, N.E. Polyakov, O.Y. Selyutina, T.G. Tolstikova, T.S. Frolova, V.A. Mordvinov, A.V. Dushkin, N.Z. Lyakhov, Disodium salt of glycyrrhizic acid – a novel supramolecular delivery system for anthelmintic drug praziquantel, J. Drug Delivery Sci. Technol. 50 (2019) 66–77, https://doi.org/10.1016/j.jddst.2019.01.014.

[15] V.A. Vavilin, N.F. Salakhutdinov, Y.I. Ragino, N.E. Polyakov, M.B. Taraban, T.V. Leshina, E.M. Stakhneeva, V.V. Lyakhovich, Y.P. Nikitin, G.A. Tolstikov, Hypocholesteremic properties of complex compound of simvastatin with glycyrrhizic acid (simvaglizin) in experimental models, Biomed. Chem. 54 (2008) 301–313, https://doi.org/10.1134/S1990750808040070.

[16] B. Li, P. Vachali, Z. Shen, A. Gorusupudi, K. Nelson, B. Besch, A. Bartschi, S. Longo, T. Mattinson, S. Shihab, L. Suntsova, A. Dushkin, N. Polyakov, P. Bernstein, Retinal Accumulation of Zeaxanthin, Lutein, and β-Carotene in Mice Deficient in Carotenoid Cleavage Enzymes, Exp. Eye Res. 159 (2017) 123–131, https://doi.org/10.1016/j.exer.2017.02.016.

[17] Q. Zhang, N.E. Polyakov, Y.S. Chistyachenko, M.V. Khvostov, T.S. Frolova, T.G. Tolstikova, A.V. Dushkin, S.u. Weike, Preparation of curcumin self-micelle solid dispersion with enhanced bioavailability and cytotoxic activity by mechanochemistry, Drug Delivery 25 (1) (2018) 198–209, https://doi.org/10.1080/10717544.2017.1422298.

[18] R. Kong, X. Zhu, E.S. Meteleva, Y.S. Chistyachenko, L.P. Suntsova, N.E. Polyakov, M.V. Khvostov, D.S. Baev, T.G. Tolstikova, J. Yu, A.V. Dushkin, W. Su, Enhanced solubility and bioavailability of simvastatin by mechanochemically obtained complexes, Int. J. Pharm. 534 (1-2) (2017) 108–118, https://doi.org/10.1016/j.ijpharm.2017.10.011.

[19] N.E. Polyakov, T.V. Leshina, N.F. Salakhutdinov, L.D. Kispert, Host-Guest Complexes of Carotenoids with β-Glycyrrhizic Acid, J. Phys. Chem. 110 (13) (2006) 6991–6998, https://doi.org/10.1021/jp056038l.

[20] N.E. Polyakov, V.K. Khan, M.B. Taraban, T.V. Leshina, Complex of Calcium Receptor Blocker Nifedipine with Glycyrrhizic Acid, J. Phys. Chem. B. 112 (14) (2008) 4435–4440, https://doi.org/10.1021/jp076850j.

[21] N.E. Polyakov, A. Magyar, L.D. Kispert, Photochemical and Optical Properties of Water-Soluble Xanthophyll Antioxidants: Aggregation vs Complexation, J. Phys. Chem. B. 117 (35) (2013) 10173–10182, https://doi.org/10.1021/jp4062708.

[22] I.E. Apanasenko, O.Y. Selyutina, N.E. Polyakov, L.P. Suntsova, E.S. Meteleva, A.V. Dushkin, P. Vachali, P.S. Bernstein, Solubilization and stabilization of macular carotenoids by water soluble oligosaccharides and polysaccharides, Archives of Biochemistry and Biophysics - 572 (2015) 58–65, https://doi.org/10.1016/j.abb.2014.12.010.

[23] V.S. Kornievskaya, A.I. Kruppa, N.E. Polyakov, T.V. Leshina, Effect of glycyrrhizic acid on lappaconitine phototransformation, J. Phys. Chem. 111 (39) (2007) 11447–11452, https://doi.org/10.1021/jp0739770.

[24] S.S. Petrova, A.A. Schlotgauer, A.I. Kruppa, T.V. Leshina, Self-Association of Glycyrrhizic Acid. NMR Study, Zeitschrift für Physikalische Chemie – 231 (2016) 1–17, https://doi.org/10.1515/zpch-2016-0845.

[25] A.V. Dushkin, E.S. Meteleva, T.G. Tolstikova, M.V. Khvostov, N.E. Polyakov, N.Z. Lyakhov, Supramolecular Systems for the Delivery of the Molecules of Medicinal Substances Based on Water-Soluble Plant Metabolites. Physicochemical, Pharmacological Properties and the Features of Mechanochemical Preparation, Chem. Sustain. Dev. 27 (2019) 206–216, https://doi.org/10.15372/CSD2019129.

[26] S.N. Borisenko, E.V. Vetrova, A.A. Milov, E.V. Vetrova, N.I. Borisenko, Mass-spectrometry and Quantum-chemical study of self-association processes of glycyrrhizinic acid molecules, Chem. Plant Mater. 2 (2013) 85–92, https://doi.org/10.14258/jcprm.1321085) (in Russian.

[27] A.V. Lekar, E.V. Vetrova, N.I. Borisenko, L.A. Yakovishin, V.I. Grishkovets, S.N. Borisenko, A mass spectrometry study of the self-association of glycyrrhetinic acid molecules, Russ J. Bioorg. Chem. 42 (2016) 716–720, https://doi.org/10.1134/S1068162016070037.

[28] O.Y. Selyutina, I.E. Apanasenko, A.V. Kim, E.A. Shelepova, S.S. Khalikov, N.E. Polyakov, Spectroscopic and molecular dynamics characterization of glycyrrhizin membrane-modifying activity, Colloids and surfaces, B, Biointerf. 147 (2016) 459–466, https://doi.org/10.1016/j.colsurfb.2016.08.037.

[29] O.Y. Selyutina, N.E. Polyakov, D.V. Korneev, B.N. Zaitsev, Influence of glycyrrhizin on permeability and elasticity of cell membrane: perspectives for drugs delivery, Drug Delivery 23 (3) (2016) 858–865, https://doi.org/10.3109/10717544.2014.919544.

[30] O.Y. Selyutina, I.E. Apanasenko, A.G. Shilov, S.S. Khalikov, N.E. Polyakov, Effect of natural polysaccharides and oligosaccharides on the permeability of cell membranes, Russian Chem. Bullet. Int. Ed. 66 (1) (2017) 129–135, https://doi.org/10.1007/s11172-017-1710-2.

[31] O.Y. Selyutina, I.E. Apanasenko, N.E. Polyakov, Membrane-modifying activity of glycyrrhizic acid, Russian Chem. Bullet. Int. Ed. 64 (7) (2015) 1555–1559, https://doi.org/10.1007/s11172-015-1040-1.

[32] A.V. Kim, E.A. Shelepova, O.Y. Selyutina, E.S. Meteleva, A.V. Dushkin, N.N. Medvedev, N.E. Polyakov, N.Z. Lyakhov, Glycyrrhizin-assisted transport of praziquantel anthelmintic drug through the lipid membrane: an experiment and MD simulation, Mol. Pharm. 16 (7) (2019) 3188–3198, https://doi.org/10.1021/acs.molpharmaceut.9b00390.

[33] O.Y. Selyutina, A.V. Mastova, E.A. Shelepova, N.E. Polyakov, pH-Sensitive Glycyrrhizin Based Vesicles for Nifedipine Delivery, Molecules 26 (5) (2021) 1270, https://doi.org/10.3390/molecules26051270.

[34] P. Berben, A. Bauer-Brandl, M. Brandl, B. Faller, G.E. Flaten, A.-C. Jacobsen, J. Brouwers, P. Augustijns, Drug permeability profiling using cell-free permeation tools: Overview and applications, European Journal of Pharmaceutical Sciences 119 (2018) 219–233, https://doi.org/10.1016/2018.04.016.

[35] Jurgen Mensch, Anouche Melis, Claire Mackie, Geert Verreck, Marcus E. Brewster, Patrick Augustijns, Evaluation of various PAMPA models to identify the most discriminating method for the prediction of BBB permeability, Eur. J. Pharm. Biopharm. 74 (3) (2010) 495–502, https://doi.org/10.1016/j.ejpb.2010.01.003.

[36] M. Kansy, F. Senner, K. Gubernator, Physicochemical high throughput screening: parallel artificial membrane permeation assay in the description of passive absorption processes, J Med Chem. 41 (7) (1998) 1007–1010, https://doi.org/10.1021/jm970530e.

[37] B.J. Bennion, N.A. Be, M.W. McNerney, Victoria Lao, E.M. Carlson, C.A. Valdez, M.A. Malfatti, H.A. Enright, T.H. Nguyen, F.C. Lightstone, T.S. Carpenter, Predicting a Drug's Membrane Permeability: A Computational Model Validated With in Vitro Permeability Assay Data, J. Phys. Chem. B 121 (20) (2017) 5228–5237, https://doi.org/10.1021/acs.jpcb.7b0291410.1021/acs.jpcb.7b02914.s001.

[38] M. Krstić, M. Popović, V. Dobričić, S. Ibrić, Influence of Solid Drug Delivery System Formulation on Poorly Water-Soluble Drug Dissolution and Permeability, Molecules 20 (2015) 14684–14698, https://doi.org/10.3390/molecules200814684.

[39] Alfredo E. Cardenas, Gouri S. Jas, Kristine Y. DeLeon, Wendy A. Hegefeld, Krzysztof Kuczera, Ron Elber, Unassisted Transport of N-Acetyl-L-tryptophanamide through Membrane: Experiment and Simulation of Kinetics, J. Phys. Chem. B 116 (2012) 2739–2750, https://doi.org/10.1021/jp2102447.

[40] E.S. Meteleva, V.I. Evseenko, O.I. Teplyakova, S.S. Khalikov, N.E. Polyakov, I.E. Apanasenko, A.V. Dushkin, N.G. Vlasenko, Nanopesticides on the Basis of the Supramolecular Complexes of Tebuconazole for the Treatment of Seeds of Cereals, Chem. Sustain. Develop. 3 (2018) 279–294, https://doi.org/10.15372/CSD20180304.

[41] M. Bermejo, A. Avdeef, A. Ruiz, R Nalda, J.A. Ruell, O. Tsinman, I. González, C. Fernández, G. Sánchez, T.M. Garrigues, V. Merino, PAMPA-a drug absorption in vitro model. 7. Comparing rat in situ, Caco-2, and PAMPA permeability of fluoroquinolones, European Journal of Pharmaceutical Sciences 21 (2004) 429–441. https://doi.org/10.1016/j.ejps.2003.10.009.

[42] W. Shirley, I. Siu, R. Vácha, P. Jungwirth, R.A. Böckmann, Biomolecular simulations of membranes: physical properties from different force fields, J. Chem. Phys. 128 (2008) https://doi.org/10.1063/1.2897760 125103.

[43] A.K. Malde, L. Zuo, Matthew Breeze, Martin Stroet, David Poger, Pramod C. Nair, Chris Oostenbrink, Alan E. Mark, An Automated force field Topology Builder (ATB) and repository: version 1.0, J. Chem. Theory Comput. 7 (12) (2011) 4026–4037, https://doi.org/10.1021/ct200196m.

[44] H.J.C. Berendsen, J.P.M. Postma, W.F. van Gunsteren, J. Hermans, Interactionmodels for water in relation to protein hydration, Reidel: Dordrecht (1981) 331–342, https://doi.org/10.1007/978-94-015-7658-1_21.

[45] Shankar Kumar, John M. Rosenberg, Djamal Bouzida, Robert H. Swendsen, Peter A. Kollman, The weighted histogram analysis method for free-energy calculations on biomolecules I. The method, J. Comp. Chem. 13 (8) (1992) 1011–1021, https://doi.org/10.1002/(ISSN)1096-987X10.1002/jcc.v13:810.1002/jcc.540130812.

[46] M.R. Shirts, D.L. Mobley, An introduction to best practices in free energy calculations, Biomol. Simulat. Meth. Protocols (2013) 271–311, https://doi.org/10.1007/978-1-62703-017-5_11.

[47] G.M. Torrie, J.P. Valleau, Nonphysical sampling distributions in Monte Carlo free-energy estimation: Umbrella sampling, J. Comp. Phys. 23 (2) (1977) 187–199, https://doi.org/10.1016/0021-9991(77)90121-8.

[48] Timothy S. Carpenter, Daniel A. Kirshner, Edmond Y. Lau, Sergio E. Wong, Jerome P. Nilmeier, Felice C. Lightstone, A Method to Predict Blood-Brain Barrier Permeability of Drug-Like Compounds Using Molecular Dynamics Simulations, Biophys. J. 107 (3) (2014) 630–641, https://doi.org/10.1016/j.bpj.2014.06.024.

[49] Siewert-Jan Marrink, Herman J.C. Berendsen, Simulation of water transport through a lipid membrane, J. Phys. Chem. 98 (15) (1994) 4155–4168, https://doi.org/10.1021/j100066a040.

[50] G. Hummer, Position-dependent diffusion coefficients and free energies from Bayesian analysis of equilibrium and replica molecular dynamics simulations, New J. Phys. 7 (2005) 34, https://doi.org/10.1088/1367-2630/7/1/034.

[51] Ekaterina A. Shelepova, Alexandra V. Kim, Vladimir P. Voloshin, Nikolai N. Medvedev, Intermolecular voids in lipid bilayers in the presence of glycyrrhizic acid, J. Phys. Chem. B 122 (43) (2018) 9938–9946, https://doi.org/10.1021/acs.jpcb.8b0798910.1021/acs.jpcb.8b07989.s001.

[52] Susruta Samanta, Samira Hezaveh, Giuseppe Milano, Danilo Roccatano, Diffusion of 1,2-Dimethoxyethane and 1,2-Dimethoxypropane through Phosphatidycholine Bilayers: A Molecular Dynamics Study, J. Phys. Chem. B 116 (17) (2012) 5141–5151, https://doi.org/10.1021/jp211564x.